The plagioclase, forsterite, diopside, liquid equilibrium in the system CaO–Na$_2$O–MgO–Al$_2$O$_3$–SiO$_2$

G. M. Biggar and D. J. Humphries

Department of Geology, University of Edinburgh, West Mains Road, Edinburgh, EH9 3JW

ABSTRACT. Liquids in the system CaO–Na$_2$O–MgO–Al$_2$O$_3$–SiO$_2$ which crystallize plagioclase and forsterite, often with diopside and sometimes with spinel, were studied. The movement of the plagioclase–forsterite saturation surface to higher plagioclase contents as albite replaces anorthite, and the concurrent expansion of the forsterite and diopside primary fields, are documented. The maximum temperature of the liquid in equilibrium with plagioclase, diopside, and forsterite decreases as the anorthite to albite ratio decreases and as enstatite is added, and was experimentally determined over part of its range from 1278 to 1130 °C. The decrease was not linear, being generally small even when 67 mole % albite was present, and thereafter, it must decrease rapidly to reach the values reported for the system albite–diopside–forsterite.

PLAGIOCLASE, olivine, and augite are common phenocrysts in basalts but require at least the six component system CaO–Na$_2$O–MgO–FeO–Al$_2$O$_3$–SiO$_2$ for representation. The simpler soda- and iron-free system anorthite–diopside–forsterite–silica has been extensively studied and its application to basalt petrogenesis discussed (e.g. Cox et al., 1979, pp. 210 et seq.). With soda present the join albite–diopside–forsterite is known (Schairer and Morimoto, 1959) but data at intermediate Ca:Na ratios and for the addition of enstatite are few (see fig. 5). The present paper documents some of the changes in the plagioclase–olivine crystallization surface as An:Ab changes, and as the bulk composition changes from zero to 25% enstatite in the norm.

The anorthite–forsterite crystallization surface is shown in fig. 1B. It is bounded by the four-phase equilibria; Fo–An–Di–Lq represented by the curve a_1–p_1 to which most of the data in this paper refer; Fo–An–Sp–Lq represented by the curve b_1–c_1, for which a few data are presented; and Fo–An–En–Lq, the curve d_1–p_1, which was not encountered. The crystallization surface also extends beyond the tetrahedron shown in fig. 1B into other regions of CaO–MgO–Al$_2$O$_3$–SiO$_2$ space.

Experimental methods and results. Compositions were synthesized by the 'gel' technique (Biggar and O'Hara, 1969a) and equilibrated in batches of twelve in platinum capsules (Biggar and O'Hara, 1969b) for periods of at least 168 hours and up to 336 hours in some experiments. Temperatures were referenced to a scale based on melting-points of gold (1064.5 °C), lithium metasilicate (1208 °C), and diopside (1395 °C) (Biggar, 1972). The products were identified by optical microscopy. The experimental details were reported by Humphries (1975), and the compositions and results are shown in Tables I–III.

The compositions lay on joins from diopside to the points K, L and M as shown in fig. 1, the legend of which gives the molar compositions. Each of these joins was studied at four different molar feldspar compositions, An:An$_2$Ab$_1$; AnAb:An$_1$Ab$_2$. The soda-bearing compositions were recalculated for projections and diagrams according to a scheme used by O'Hara (1976) which ensures that albite plots as its molar equivalent of anorthite (see also Cox et al., 1979, p. 245).

The experimental data were used to construct fig. 2 for the joins K, L, and M, respectively, at several anorthite to albite ratios as noted. These show the temperature of appearance of the second crystalline phase (after primary forsterite). Data for the plagioclase, forsterite, diopside, liquid locus are sufficient to fix its position in the diagrams but the plagioclase, forsterite, spinel, liquid locus is less well fixed, particularly in figs. 2A and B, since most of the data lie in Fo–Plag–Lq and few data lie in Fo–Sp–Lq.

A second series of diagrams (figs. 3A to F) shows the same data used to deduce the nature of the forsterite projection on to the plane CaSiO$_3$–MgSiO$_3$–Al$_2$O$_3$. These forsterite projections show clearly the Fo–Plag–Lq surface, contoured for the temperature of appearance of plagioclase. This surface decreases in size and moves to more

FIG. 1. Fig. A is a distorted version of the CaO–MgO–Al_2O_3–SiO_2 tetrahedron to show the sub-tetrahedron FO–AN–DI–S of fig. B. The compositions studied lie on three joins; diopside to $MgAl_2SiO_6$ (magnesian tschermaks molecule) shown as MAS and this join intersects anorthite–forsterite at the point labelled K; diopside to $Mg_5Al_6S_5O_{24}$ shown as $M_5A_3S_5$, which intersects An–Fo–SiO_2 at point L; and diopside to $Mg_7Al_6S_7O_{30}$ which intersects An–Fo–SiO_2 at point M. The plane enstatite–wollastonite–alumina (MS–CS–A) fig. A, contains all the compositions studied.

Fig. B shows the anorthite–diopside–forsterite–silica tetrahedron (similar labels to Presnall et al., 1978) with the anorthite–forsterite crystallization surface shown as a stippled area. The compositions studied experimentally lie on the joins Di–K, Di–L, Di–M, but to avoid confusion the actual compositions are only schematically represented as filled circles on one of these joins, Di–L. For completeness, note that K has the molar composition AnFo which is CAM_2S_3; L is $AnFoEn_{0.66}$ which is $C_3A_3M_8S_{11}$; M is $AnFoEn_{1.33}$ which is $C_3A_3M_{10}S_{13}$; and in figs. 2, 3, and 4, the equivalent points, for example when anorthite is replaced by An_2Ab_1 are shown as K_1, L_1, and M_1. The dashed boundaries a^1–p^1–d^1 illustrate the movement of the plagioclase–forsterite crystallization surface closer to the plagioclase apex as observed in the experiments and shown in subsequent figures.

Table I. Compositions (in moles) studied in the system Cao-MgO-Al_2O_3-SiO_2

Code	*	CaO	MgO	Al_2O_3	SiO_2	Code		CaO	MgO	Al_2O_3	SiO_2	Code		CaO	MgO	Al_2O_3	SiO_2
H13	K	1.5	2.5	1.0	4.0	H17	L	3.75	8.75	3.0	12.5	H21	M	3.75	10.75	3.0	14.5
H14	K	2.0	3.0	1.0	5.0	H18	L	5.25	10.25	3.0	15.5	H22	M	5.25	12.25	3.0	17.5
H4	K	2.375	3.375	1.0	5.75	H1	L	6.5	11.5	3.0	18.0	H23	M	6.0	13.0	3.0	19.0
H5	K	2.5	3.5	1.0	6.0	H2	L	7.0	12.0	3.0	19.0	H24	M	6.75	13.75	3.0	20.5
H6	K	2.625	3.625	1.0	6.25	H3	L	7.5	12.5	3.0	20.0	H25	M	7.5	14.5	3.0	22.0
H15	K	3.0	4.0	1.0	7.0	H19	L	9.0	14.0	3.0	23.0	H26	M	9.0	16.0	3.0	25.0
H16	K	4.0	5.0	1.0	9.0	H20	L	12.0	17.0	3.0	29.0	H27	M	12.0	19.0	3.0	31.0

* The first part of the code identifies each compositon, the second part, K, L, M, etc identifies the lines from diopside in figs. 2, 3, and 4.

Table II. Compositions (in moles) studied in the system CaO-Na_2O-Al_2O_3-SiO_2

Code		CaO	MgO	Al_2O_3	SiO_2	Na_2O	Code		CaO	MgO	Al_2O_3	SiO_2	Na_2O	Code		CaO	MgO	Al_2O_3	SiO_2	Na_2O
N19	K1	1.25	3.25	1.25	5.5	0.25	N20	L1	1.0	4.0	1.25	6.0	0.25	N23	M1	0.66	4.666	1.25	6.333	0.25
N16	K1	1.5	3.5	1.25	6.0	0.25	N10	L1	1.5	4.5	1.25	7.0	0.25	N24	M1	1.25	5.25	1.25	7.5	0.25
N1	K1	1.875	3.875	1.25	6.75	0.25	N11	L1	1.75	4.75	1.25	7.5	0.25	N25	M1	1.5	5.5	1.25	8.0	0.25
N2	K1	2.0	4.0	1.25	7.0	0.25	N12	L1	2.0	5.0	1.25	8.0	0.25	N26	M1	1.75	5.75	1.25	8.5	0.25
N3	K1	2.25	4.25	1.25	7.5	0.25	N21	L1	2.5	5.5	1.25	9.0	0.25	N27	M1	2.25	6.25	1.25	9.5	0.25
N17	K1	3.0	5.0	1.25	9.0	0.25	N22	L1	3.5	6.0	1.25	11.0	0.25	N28	M1	3.0	7.0	1.25	11.0	0.25
N18	K1	4.0	6.0	1.25	11.0	0.25													
L19	K2	1.25	4.25	1.5	7.5	0.5	L22	L2	1.5	14.5	4.5	22.5	1.5	L26	M2	1.0	18.0	4.5	25.0	1.5
L1	K2	1.75	4.75	1.5	8.5	0.5	L23	L2	2.5	15.5	4.5	24.0	1.5	L27	M2	2.0	19.0	4.5	27.0	1.5
L2	K2	2.0	5.0	1.5	9.0	0.5	L16	L2	3.5	16.5	4.5	26.0	1.5	L28	M2	3.0	20.0	4.5	29.0	1.5
L3	K2	2.25	5.25	1.5	9.5	0.5	L17	L2	4.5	17.5	4.5	28.0	1.5	L29	M2	3.75	20.75	4.5	30.5	1.5
L20	K2	3.0	6.0	1.5	11.0	0.5	L18	L2	5.5	18.5	4.5	30.0	1.5	L30	M2	4.5	21.5	4.5	32.0	1.5
L21	K2	4.0	7.0	1.5	13.0	0.5	L24	L2	7.0	20.0	4.5	33.0	1.5	L31	M2	6.0	23.0	4.5	35.0	1.5
							L25	L2	10.0	23.0	4.5	39.0	1.5	L32	M2	9.0	26.0	4.5	41.0	1.5
A16	K3	1.0	6.0	2.0	11.0	1.0	A19	L3	0.5	7.5	2.0	12.0	1.0	A23	M3	0.5	9.5	2.0	14.0	1.0
A1	K3	1.5	6.5	2.0	12.0	1.0	A10	L3	1.0	8.0	2.0	13.0	1.0	A25	M3	1.5	10.5	2.0	16.0	1.0
A2	K3	2.0	7.0	2.0	13.0	1.0	A11	L3	1.25	8.25	2.0	13.5	1.0	A27	M3	3.0	12.5	2.0	19.0	1.0
A3	K3	2.375	7.375	2.0	13.75	1.0	A12	L3	1.5	8.5	2.0	14.0	1.0						
A18	K3	3.5	8.5	2.0	16.0	1.0	A20	L3	2.0	9.0	2.0	15.0	1.0						
A17	K3	5.0	10.0	2.0	19.0	1.0	A21	L3	3.0	10.0	2.0	17.0	1.0						
							A22	L3	4.0	11.0	2.0	19.0	1.0						

Table III. Experimental temperatures and products

Code	°C	Phases
H13 K	1278	fo an lq
	1264	fo an di lq
H14 K	1280	fo an di lq
H4 K	1306	fo lq
	1292	fo lq
	1286	fo lq
	1280	fo an di lq
	1274	fo an di lq
H5 K	1306	fo lq
	1292	fo lq
	1286	fo lq
	1280	fo an di lq
	1274	fo an di lq
H6 K	1306	fo lq
	1292	fo lq
	1286	fo lq
	1280	fo an di lq
	1274	fo an di lq
H15 K	1280	fo an di lq
H16 K	1280	fo an di lq
H17 L	1278	fo an lq
	1264	fo an lq
H18 L	1280	fo an di lq
H1 L	1306	fo lq
	1292	fo lq
	1286	fo lq
	1280	fo an di lq
	1274	fo an di lq
	1263	fo an di lq
L19 K2	1274	fo pl lq
	1251	fo pl lq
	1239	fo pl lq
	1229	fo pl di lq
L1 K2	1274	fo lq
	1257	fo pl lq
	1251	fo pl lq
	1241	fo pl lq
	1239	fo pl di lq
L2 K2	1274	fo lq
	1257	fo pl lq
	1251	fo pl lq
	1241	fo pl di lq
	1239	fo pl di lq
L3 K2	1274	fo lq
	1257	fo lq
	1251	fo pl lq
	1245	fo pl lq
	1241	fo pl di lq
	1239	fo pl di lq
L20 K2	1274	fo lq
	1251	fo di lq
	1245	fo di lq
	1239	fo pl di lq
L21 K2	1251	fo di lq
	1239	fo pl di lq
L22 L2	1245	fo sp lq
	1229	fo sp lq
L23 L2	1251	fo pl sp lq

Code	°C	Phases
H2 L	1306	fo lq
	1292	fo lq
	1286	fo lq
	1280	fo an di lq
	1274	fo an di lq
	1263	fo an di lq
H3 L	1306	fo lq
	1292	fo lq
	1286	fo lq
	1280	fo an di lq
	1274	fo an di lq
	1263	fo lq
H19 L	1280	fo an di lq
H20 L	1280	fo di lq
H21 M	1278	fo an lq
H22 M	1278	fo an lq
	1264	fo an lq
H23 M	1278	fo an lq
	1264	fo an di lq
H24 M	1278	fo lq
	1264	fo an di lq
H25 M	1278	fo an di lq
	1264	fo an di lq
H26 M	1278	fo di lq
	1264	fo an di lq
H27 M	1278	fo di lq
	1264	fo an di lq
L16 L2	1274	fo lq
	1251	fo pl lq
	1245	fo pl lq
	1239	fo pl lq
	1229	fo pl di lq
L17 L2	1251	fo pl lq
	1239	fo pl lq
	1229	fo pl di lq
L18 L2	1251	fo lq
	1245	fo lq
	1239	fo pl di lq
L24 L2	1274	fo lq
	1251	fo di lq
	1239	fo pl di lq
L25 L2	1274	fo di lq
	1251	fo di lq
	1239	fo pl di lq
L26 M2	1245	fo, sp lq
L27 M2	1245	fo sp lq
L28 M2	1245	fo pl lq
	1229	fo pl px lq
L29 M2	1245	fo pl lq
	1229	fo pl px lq
L30 M2	1245	fo pl di lq
	1229	fo pl di lq
L31 M2	1245	fo lq
	1229	fo pl di lq
L32 M2	1229	fo pl di lq

Code	°C	Phases
N19 K1	1274	fo pl lq
	1250	fo pl lq
N16 K1	1274	fo pl lq
	1250	fo pl lq
	1242	fo pl lq
N1 K1	1247	fo pl lq
	1263	fo pl lq
	1260	fo pl lq
	1251	fo pl lq
	1242	fo pl di lq
	1234	fo pl di lq
N2 K1	1263	fo lq
	1260	fo pl lq
	1251	fo pl lq
	1242	fo pl di lq
	1234	fo pl di lq
N3 K1	1263	fo lq
	1260	fo lq
	1251	fo pl di lq
	1242	fo pl di lq
	1234	fo pl di lq
N17 K1	1274	fo di lq
	1260	fo di lq
	1242	fo pl di lq
N18 K1	1242	fo pl di lq
N20 L1	1274	fo pl lq
	1250	fo pl px lq
	1242	fo pl px lq
N10 L1	1274	fo pl lq
	1263	fo pl lq
	1260	fo pl lq
	1251	fo pl lq
	1242	fo pl lq
	1234	fo pl di lq
A16 K3	1234	fo pl lq
A1 K3	1234	fo pl lq
	1222	fo pl lq
	1213	fo pl di lq
	1205	fo pl di lq
A2 K3	1246	fo lq
	1234	fo pl lq
	1227	fo pl di lq
	1222	fo pl di lq
	1213	fo pl di lq
	1205	fo pl di lq
A3 K3	1246	fo lq
	1234	fo di lq
	1227	fo pl di lq
	1222	fo pl di lq
	1213	fo pl di lq
	1205	fo pl di lq
A18 K3	1234	fo di lq
A17 K3	1234	fo di lq
A19 L3	1234	fo sp lq
	1227	fo sp lq
A10 L3	1246	fo pl lq
	1234	fo pl lq
	1227	fo pl px lq
	1213	fo pl px lq

Code	°C	Phases
N11 L1	1274	fo lq
	1263	fo pl lq
	1260	fo pl lq
	1251	fo pl lq
	1250	fo pl di lq
	1242	fo pl di lq
N12 L1	1234	fo pl di lq
	1263	fo lq
	1260	fo pl lq
	1251	fo pl lq
	1250	fo pl di lq
	1242	fo pl di lq
N21 L1	1234	fo pl di lq
	1274	fo di lq
	1260	fo di lq
	1242	fo pl di lq
N22 L1	1274	fo di lq
	1250	fo pl di lq
	1242	fo pl di lq
N23 M1	1250	fo pl sp lq
N24 M1	1274	fo pl lq
	1260	fo pl lq
	1250	fo pl lq
N25 M1	1274	fo pl lq
	1260	fo pl lq
	1250	fo pl lq
N26 M1	1274	fo lq
	1260	fo pl lq
	1250	fo pl lq
N27 M1	1260	fo di lq
	1250	fo pl di lq
N28 M1	1274	fo di lq
	1250	fo pl di lq
A11 L3	1246	fo pl lq
	1234	fo pl lq
	1227	fo pl px lq
	1222	fo pl px lq
	1213	fo pl px lq
	1205	fo pl px lq
A12 L3	1246	fo lq
	1234	fo pl lq
	1227	fo pl px lq
	1222	fo pl px lq
	1213	fo pl px lq
	1205	fo pl px lq
A20 L3	1246	fo lq
	1234	fo pl lq
	1227	fo pl lq
	1213	fo pl di lq
A21 L3	1246	fo di lq
	1234	fo di lq
A23 M3	1246	fo sp lq
A25 M3	1246	fo pl lq
	1227	fo pl lq
	1213	fo pl lq
A27 M3	1246	fo di lq
	1227	fo di lq
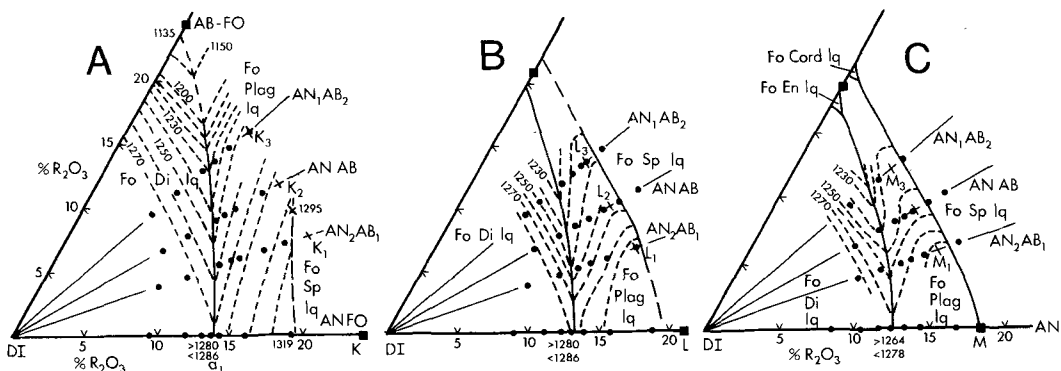
FIG. 2A, B, and C. Experimental data for joins of the type diopside-K, diopside-L, etc. with similar joins to L_1, L_2 etc., in which anorthite is replaced, in steps, by albite. The compositions studied are shown as filled circles, and the data from Tables I–III are used to construct the contours. These are not liquidus contours, since all the samples had forsterite as liquidus phase at some higher, undetermined temperature, but they are contours for the appearance of the second crystalline phase, usually plagioclase or diopside. In a few cases when there was a high albite and high enstatite content in the starting material, for example close to M_3 in C, the pyroxene in the experimental charge is shown as px (in the tables) to indicate uncertainty about its identification as augite. It may be pigeonite or a mixture of pigeonite and augite. The diagrams are drawn for the assumption that it was augite. Data for the Di–Ab–Fo join are from Schairer and Morimoto (1959). An early version of fig. 2A was published by Humphries (1972).
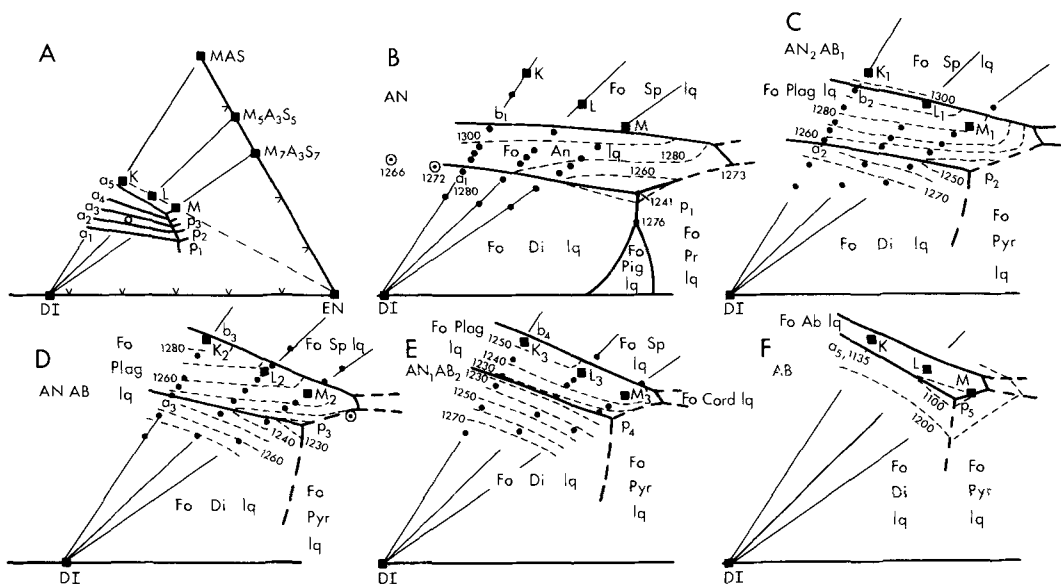
FIG. 3. Forsterite projections into the plane Woll–En–Al_2O_3 (CS–MS–A) shown in fig. 1A. Fig. 3A is a location diagram for the joins studied (see also fig. 1) and fig. 3A is also a summary diagram, the curves a_1–p_1, a_2–p_2 etc. derive from figs. 3B to F which show, at greater scale, details of the Fo–Plag–Lq field. Contours (at 20 °C in fig. 3B, otherwise at 10 °C, except fig. 3F) are drawn as best fits to the data in the tables for the compositions shown as filled circles. K, L, M, etc., serve as cross-reference points between the figures. In fig. 3B the two circles at 1266 °C and 1272 °C are projections of liquid compositions from microprobe analyses by Presnall et al. (1978). The nature of the calcium-poor pyroxene phases shown in fig. B as Pr (for protoenstatite) is uncertain in the light of the recent finding of orthopyroxene in the join enstatite-diopside (Longhi and Boudreau 1980). The open circle (fig. A) represents the position of the Ol, $An_{60}Ab_{40}$, Di, boundary at 1235 ± 5 °C from Emslie (1971) in agreement (to better than 10 °C) with the present data. The open circle (fig. D) is the forsterite projection of an analysis by Eggler (1974) of a liquid at 1228 °C in equilibrium with forsterite, plagioclase, calcium-poor pyroxene (from a composition with a normative $An_{50}Ab_{50}$), and it also agrees with the present data (1240 °C by interpolation).
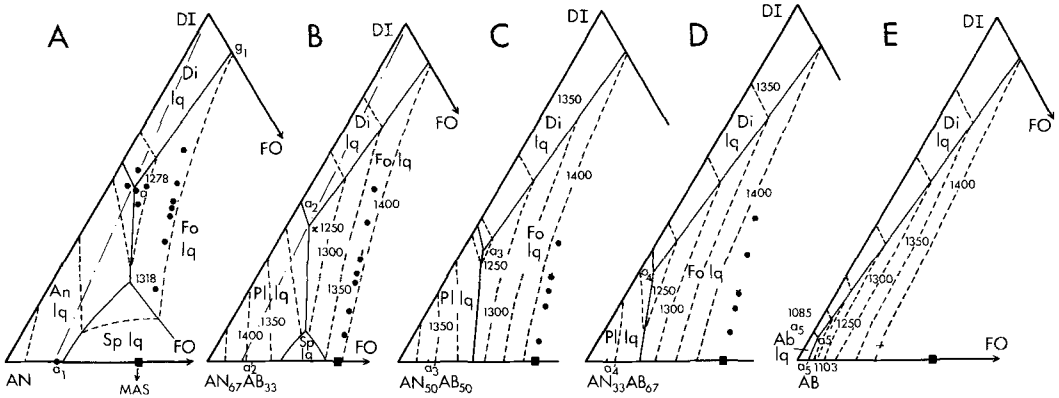
FIG. 4A to E. Estimates of phase diagrams in diopside–forsterite–plagioclase based on data from joins of the type Diopside–K (and in fig. A extra data from points near the anorthite forsterite diopside field boundary). Estimates of the temperatures of the points where the plagioclase, diopside, and olivine fields meet are given in fig. 5.

aluminous compositions as albite replaces anorthite, and temperatures on these successive surfaces drop.

To more clearly illustrate the manner in which the plagioclase field contracts and the fields of diopside and forsterite expand as Na:Ca increases, the diagrams in fig. 4 were constructed. Along this series the temperature of the feldspar, diopside, forsterite, liquid equilibrium (points a_1 to a_5) decrease (details summarized in fig. 5). Further, but smaller, temperature decrease occurs as enstatite is added (see also fig. 5). The most striking feature (also seen in fig. 2A) is that increasing albite has relatively little effect on temperature until the albite content is above 67% after which there must be a more rapid drop in temperature down to the values for the join diopside–albite–forsterite.

The behaviour of the equilibrium involving spinel with feldspar and olivine is less well docu-

mented, but at some point between fig. 3C and D the forsterite, spinel, liquid field no longer covers the point K, that is the locus of the points b_1, b_2, b_3 crosses the point K. Spinel is no longer in reaction relation with the liquid. Fig. 6 illustrates this feature and leads to an estimate of $An_{59}Ab_{41}$ for the change from spinel reaction to spinel precipitation in the equilibrium plagioclase–forsterite–spinel–liquid.

Conclusion. The basic forms of the diagrams presented have been known and well used by petrologists in past discussions of basaltic petrogenesis and differentiation. The present data for plagioclase, diopside, forsterite, liquid provide some temperature information and show a very non-linear slow decrease in temperature up to high albite contents, followed by a rapid decrease of temperature.
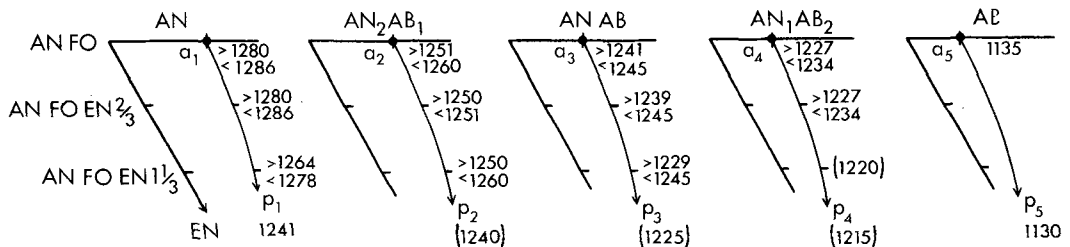
FIG. 5. Schematic diagrams to show changes in temperature of the plagioclase, diopside, olivine, liquid equilibrium as enstatite is added and as albite replaces anorthite, based on data in the tables. The temperature of p_1 is known but temperatures of p_2, p_3, etc. at which enstatite starts to crystallize with the three other minerals are not known. The temperature of p_5 will be close to the plagioclase–diopside–forsterite piercing point at 1130 °C given by Schairer and Morimoto (1959).
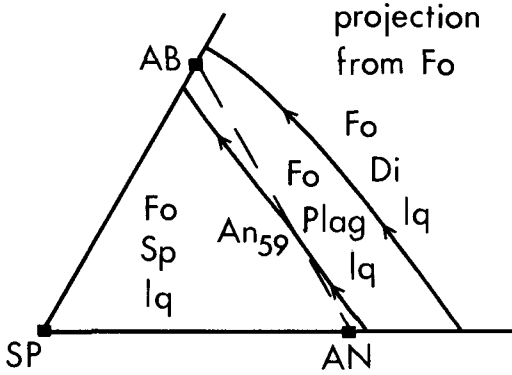
FIG. 6. Projection from forsterite on to the join spinel–anorthite–albite showing the same field boundaries as in fig. 2 and estimating that An$_{59}$ marks the change in nature from spinel reaction to spinel precipitation.

REFERENCES

Biggar, G. M. (1972). *Mineral. Mag.* **38**, 768.
—— and O'Hara, M. J. (1969*a*). Ibid. **37**, 198.
—— —— (1969*b*). Ibid. 1.
Cox, K. G., Bell, J. D., and Pankhurst, R. J. (1979). *The interpretation of igneous rocks.* George Allen & Unwin, London, 450 pp.
Eggler, D. H. (1974). *Am. J. Sci.* **274**, 297.
Emslie, R. F. (1971). *Carnegie Inst. Washington Yearb.* **69**, 148.
Humphries, D. J. (1972). *Progress in Exptl. Petrol.* 2nd Report. NERC London, Publication Series D, No. 2, p. 120.
—— (1975). *Phase equilibrium studies of some basalt-like compositions in the system CaO–MgO–Al$_2$O$_3$–SiO$_2$–Na$_2$O–Fe–O$_2$.* Thesis, University of Edinburgh.
Longhi, J. and Boudreau, A. E. (1980). *Am. Mineral.* **65**, 563.
O'Hara, M. J. (1976). *Progress in Exptl. Petrol.* 3rd Report. NERC, p. 103. London, Publication Series D, No. 6, 1976, pp. 103–26.
Presnall, D. C., Dixon, S. A., Dixon, J. R., 'Donnell, T. H., Brenner, N. L., Schrock, R. L., and Dycus, D. W. (1978). *Contrib. Mineral. Petrol.* **66**, 203.
Schairer, J. F. and Morimoto, N. (1959) *Carnegie Inst. Washington Yearb.* **58**, 113.